

15 Abstract

16 Human-mediated introductions are reshuffling species distribution on a global scale. Consequently, an
17 increasing number of allopatric taxa are now brought into contact, promoting introgressive
18 hybridization between incompletely isolated species and new adaptive gene transfer. The broadcast
19 spawning marine species, *Ciona robusta*, has been recently introduced in the native range of its sister
20 taxa, *Ciona intestinalis*, in the English Channel and North-East Atlantic. These sea squirts are highly
21 divergent, yet hybridization has been reported by crossing experiments and genetic studies in the wild.
22 Here, we examined the consequences of secondary contact between *C. intestinalis* and *C. robusta* in
23 the English Channel. We produced genomes phased by transmission to infer the history of divergence
24 and gene flow, and analyzed introgressed genomic tracts. Demographic inference revealed a history of
25 secondary contact with a low overall rate of introgression. Introgressed tracts were short, segregating
26 at low frequency, and scattered throughout the genome, suggesting traces of past contacts during the
27 last 30 ky. However, we also uncovered a hotspot of introgression on chromosome 5, characterized by
28 several hundred kb-long *C. robusta* haplotypes segregating in *C. intestinalis*, that introgressed during
29 contemporary times the last 75 years. Although locally more frequent than the baseline level of
30 introgression, *C. robusta* alleles are not fixed, even in the core region of the introgression hotspot.
31 Still, linkage-disequilibrium patterns and haplotype-based tests suggest this genomic region is under
32 recent positive selection. We further detected in the hotspot an over-representation of candidate SNPs
33 lying on a cytochrome P450 gene with a high copy number of tandem repeats in the introgressed
34 alleles. Cytochromes P450 are a superfamily of enzymes involved in detoxifying exogenous
35 compounds, constituting a promising avenue for functional studies. These findings support that
36 introgression of an adaptive allele is possible between very divergent genomes and that anthropogenic
37 hybridization can provide the raw material for adaptation of native lineages in the Anthropocene.

38 Author summary

39 Introgression, the transfer of genetic material by hybridization between taxa, is increasingly
40 recognized to sometimes persist for long periods during species divergence. However, the evolutionary
41 consequences of human-induced introgression remain largely unknown, especially in the marine
42 realm. While some argue it poses a threat to the genome integrity of native species, others consider it
43 has a great potential to fuel adaptation. In this work, we quantify the magnitude and genomic
44 distribution of introgression after secondary contact between a native sea squirt and its divergently
45 related sister species recently introduced in the English Channel. The genome-wide pattern suggests
46 introgression is mostly impeded between these two incompatible genomes. We nonetheless found a
47 hotspot of long tracts that recently introgressed in a single region of the genome, with a clear footprint
48 of recent positive selection. In the center of the hotspot, we further detected a promising candidate
49 gene for adaptive introgression: a cytochrome P450 detoxifying enzyme with a high copy number in
50 the introgressed allele. Therefore, our results support that adaptive introgression can remain possible
51 between very divergent genomes and that anthropogenic hybridization can provide the raw material
52 for the adaptation of native lineages in the Anthropocene.

53 Introduction

54 Human-mediated introductions often result in interlineage introgression (Ottenburghs 2021; North et
55 al. 2021). Pervasive introgression implies that most co-occurring introduced and native genomes of
56 sister species are still to some extent permeable to interspecific gene flow, with various outcomes from
57 genome-wide genetic swamping to adaptive introgression at few specific genomic regions (McFarlane
58 and Pemberton 2019). In the marine realm, harbors, docks and piers are prime locations for such
59 hybridization events between non-native and native lineages, sometimes resulting in singular
60 outcomes (Touchard et al. 2022). For example, Simon et al. (2020) identified a unique ecotype of
61 marine mussels in these artificial habitats (“docks mussels”), resulting from a recent admixture
62 between two closely-related European mussel species. These anthropogenic hybridizations can also
63 promote secondary contact between divergent genomes with long histories of allopatric divergence
64 (Viard et al. 2020). They provide unique opportunities to investigate the outcomes of hybridization
65 between co-occurring genetic lineages at a late stage of the speciation continuum.

66 Sea squirts are among the most critical invasive marine organisms forming a significant
67 component of the non-indigenous community in artificial marine habitats (Shenkar and Swalla 2011;
68 Zhan et al. 2015). For this reason, they were among the first marine taxa to be studied to test the
69 hypothesis of the relationship between climate change and biological invasions (Stachowicz et al.
70 2002). *Ciona robusta* is a sea squirt species native to the Northwest Pacific introduced in the early
71 2000s to the English Channel in the native range of *Ciona intestinalis* (Bouchemousse et al. 2016a).
72 The two species are found in sympatry in these regions (Nydham and Harrison 2011). However, their
73 relative abundance varies locally over seasons (Bouchemousse et al. 2016b), and they display
74 contrasting genetic diversity patterns, with low mitochondrial diversity in *C. robusta* supporting its
75 recent introduction (Bouchemousse et al. 2016a). *C. robusta* and *C. intestinalis* represent a pair of
76 species at the end of the speciation continuum with 14% of net synonymous divergence, which is well
77 above the ~2% suggested to delineate the end of the grey zone of speciation in a study of 61 pairs of
78 animal populations (Roux et al. 2016). Despite this high molecular divergence, first and second-

79 generation crosses between the two species show successful hybridization in the laboratory
80 (Bouchemousse et al. 2016b; Malfant et al. 2018). Moreover, the two species produce gametes
81 synchronously in the wild, with juveniles recruiting simultaneously (Bouchemousse et al. 2016b).
82 However, the use of >300 ancestry-informative markers on 450 individuals showed limited evidence
83 for recent hybridization in the wild, with only one F1 and no later generation hybrids found in the
84 sympatric range (Bouchemousse et al. 2016c). Therefore, efficient reproductive barriers seem to
85 restrict hybridization in nature.

86 Despite the paucity of first-generation hybrids, Le Moan et al. (2021) found compelling
87 evidence of contemporary introgression between *C. robusta* and *C. intestinalis* in the sympatric range
88 (Bay of Biscay, Iroise Sea and the English Channel) from RADseq-derived SNPs. Instead of genome-
89 wide admixture, Le Moan et al. (2021) detected a single genomic hotspot (~1.5 Mb) of long
90 introgressed *C. robusta* tracts into its native congener on chromosome 5. The absence of such
91 introgression tracts in allopatric populations suggests introgression occurred after the recent
92 introduction of *C. robusta*. At a fine spatial scale within the sympatric range, the introgressed tracts
93 displayed chaotic frequencies across sympatric localities, which has been attributed to human-
94 mediated transport among harbors (Hudson et al. 2016). The features of the introgression hotspot
95 identified between the two species, namely being *i*) unidirectional, *ii*) localized in a single genome
96 region, and *iii*) made-up of long tracts, are reminiscent of the footprint of positive selection. Therefore,
97 Le Moan et al.'s work (2021) provides a seminal example of a contemporary introgression
98 breakthrough between two species at a late stage of the speciation continuum. It underlines the need to
99 densely scan genomes with genome-wide markers, notably when considering divergent genomes that
100 may only show very localized introgression hotspots (Ravinet et al. 2018; Maxwell et al. 2019;
101 Stankowski et al. 2020; Yamasaki et al. 2020).

102 Here, we extend Le Moan et al.'s study (2021) using whole-genome sequences fully phased by
103 transmission in both *C. robusta* and *C. intestinalis* taken from their sympatric range (English Channel),
104 to *i*) specifically delineate the core region of the genomic breakthrough, *ii*) test for the footprint of
105 selection, and *iii*) identify candidate loci driving the putatively adaptive introgression. We also

106 examined a non-introgressed *Ciona roulei* population in the Mediterranean Sea, used as a control.
107 Based on experimental crosses and genome-wide analyses, recent studies showed that *C. roulei* is a
108 “Mediterranean lineage” of the accepted species *C. intestinalis*, and thus its species status needs to be
109 revised (Malfant et al. 2018; Le Moan et al. 2021). However, we will continue to name it “*C. roulei*” in
110 this study. Based on whole genomes, we recovered the observation of Le Moan et al. (2021) for a
111 genomically localized introgression breakthrough on chromosome 5 from *C. robusta* to the sympatric
112 *C. intestinalis*, absent in the *C. roulei* population of the Mediterranean Sea. We also inferred the
113 divergence history of the two species and confirmed that they have hybridized in the past, far before
114 their introduction in Europe (Roux et al. 2013). However, when including chromosome 5, we
115 recovered a signal of contemporary introgression. Next, we inferred the haplotype ancestry of the *C.*
116 *intestinalis* genomes and delineated migrant genomic tracts. In sharp contrast with a genomic
117 background interspersed with small and sparse introgressed tracts attributed to past admixture, we
118 found a distinct pattern of very long introgressed tracts segregating at intermediate frequencies at the
119 introgression hotspot on chromosome 5. Finally, using haplotype-based tests, we provided evidence
120 that the high linkage disequilibrium (LD) observed in the genomic hotspot is due to some sort of
121 positive selection. Inspecting annotated genes at the core of the introgression breakthrough, our best
122 candidate for selection was a cytochrome P450 gene, on which differentiated SNPs were over-
123 represented, and that showed a high copy number tandem repeat in the *C. robusta* introgressed
124 haplotype.

125 Results

126 Sequencing and mapping quality

127 A total of 48 whole genomes were sequenced with an average of 41M reads per individual (**Table S1**),
128 including 22 *C. intestinalis* (three were excluded due to poor sequencing), 15 *C. robusta*, 6
129 interspecific hybrids and 5 *C. roulei*. An additional 4 *C. edwardsi* individuals were sequenced to be
130 used as an outgroup, with an average of 88M reads per individual (**Table S1**). Reads were aligned
131 against the *C. robusta* reference genome (GCA_009617815.1). Differences in the mapping quality

132 were observed between species in agreement with their genetic distance to the reference (**Table S1**).
133 On average, 80% of the reads mapped in proper pair in *C. robusta*, 60% in *C. intestinalis*, 59% in *C.*
134 *roulei*, 68% in the interspecific hybrids and 44% in the outgroup *C. edwardsi*. The average depth was
135 broadly similar among species, ranging from 18X to 26X.

136 Genome-wide analysis of population structure

137 A principal component analysis on genome-wide unlinked SNPs (**Figure 1B**) showed, as expected,
138 that the *C. robusta* individuals are clearly distinguished from the *C. intestinalis* individuals sampled in
139 the sympatric populations of the English Channel (Brest and Aber Wrac'h, named 'Aber' in the
140 following text) and from the non-introgressed population of the Mediterranean Sea (Banyuls, *C.*
141 *roulei*). This primary component of genetic variation was carried by the first PCA axis (21.2% of
142 explained variance). In comparison, the second axis (6.7%) revealed a slight genetic differentiation
143 between *C. intestinalis* and *C. roulei*, validating previous findings with RADseq (Le Moan et al.
144 2021). The intraspecific F1 individuals produced in the lab (**Table S1**) fall within the genetic variance
145 of their species, while the interspecific F1s fall halfway between the two species along the first axis
146 (**Figure 1B**), validating their F1 hybrid status. The intraspecific variance along the first axis was
147 substantial within *C. intestinalis*. At the same time, this was not the case of *C. robusta* and *C. roulei*,
148 suggesting that interspecific introgression affects specifically *C. intestinalis* individuals in the English
149 Channel.

150 The SNPs contributing to species divergence on the first axis are distributed genome-wide
151 (**Figure 1C**). Still, a decline of SNP contribution on the first axis at the start of chromosome 5
152 indicated a reduction of the divergence between *C. robusta* and the sympatric *C. intestinalis*
153 populations locally in the genome. This pattern is supported by the observation of a consistently high
154 divergence across the genome between *C. robusta* and *C. intestinalis* (the maximal F_{ST} calculated in
155 non-overlapping 10 Kb windows is equal to one), except at the start of chromosome 5, where the
156 maximal F_{ST} value declined from 1 to 0.69 (**Figure S1A**). This striking decline, located between 700
157 Kb and 1.5 Mb, was not observed between *C. robusta* and *C. roulei* (**Figure S1B**). Moreover, in *C.*

158 *intestinalis*, it did not correlate with a reduction of diversity (π), suggesting it is likely due to
159 interspecific introgression rather than intraspecific selective sweeps. This pattern is very different from
160 what was observed for the averaged F_{ST} (**Figure S1**) that strongly varied across the genome. It was
161 notably higher at the beginning or in the middle of the chromosomes in regions of low intraspecific
162 genetic diversities. These large-scale averaged variations were observed in all species, indicating that
163 they may be due to the long-term effect of linked selection acting on a shared recombination landscape
164 (note that all chromosomes in *C. intestinalis* are metacentric, except chromosome 2, 7 and 8, which are
165 submetacentric (Shoguchi et al. 2006).

166 Genome-wide analysis of introgression

167 We calculated the Patterson's D statistic using *C. edwardsi* as an outgroup to test for genome-wide
168 admixture between the two species. We found evidence for an excess shared ancestry of *C. robusta*
169 with the sympatric *C. intestinalis* relative to *C. roulei* across all chromosomes (**Figure S4A**). To locate
170 introgressed genomic regions, the fraction of the genome that has been shared between species (fd)
171 was then calculated in non-overlapping windows. fd varied around zero along each chromosome
172 (**Figure S4C**), but we observed an outlying increase on chromosome 5 between 700 Kb and 1.5 Mb
173 showing a high admixture level between *C. robusta* and *C. intestinalis* (**Figure S4D**). This fd increase
174 had its maximum (25% of admixture level) centered on the introgression hotspot of chromosome 5 and
175 was only present in the sympatric range. None of the other chromosomes showed outlying genomic
176 regions, neither with *C. intestinalis*, nor with *C. roulei* (**Figure S4C**). Furthermore, the averaged per-
177 chromosome admixture proportion was weakly negatively correlated with chromosome length (**Figure**
178 **S4B**), a known proxy for the recombination rate (Kaback 1996). Such correlation is consistent with
179 higher recombination rates (shorter chromosomes) producing weaker barriers to introgression (Martin
180 and Jiggins 2017). However, chromosome 5 was a clear outlier (i.e. it has a higher fd value than
181 expected given its length).

182 We detected introgression tracts in *C. intestinalis* genomes using local ancestry inference on
183 640,044 phased SNPs and considering *C. robusta* and *C. roulei* as the parental populations. The

184 inferred tracts showed similar introgression patterns to the raw haplotypes obtained from SNPs fixed
185 between *C. robusta* and *C. roulei* (**Figure S2**). This suggests that local ancestry inferences indeed
186 detect the introgressed genomic regions while being less noisy than when considering raw haplotypes.
187 The proportion of *C. robusta* ancestry inferred was low (0.1% on average per individual), suggesting
188 that the introgression rate at the genome level is low. Furthermore, there was no significant correlation
189 in *C. robusta* ancestry between chromosomes (except in 5 pairs) among the *C. intestinalis* individuals
190 (**Table S2**). Introgressed tracts were short (median size of 380 bp) and widespread across the genome
191 (**Figure 2**). These short tracts had a bimodal frequency distribution with a majority segregating at low
192 frequency and a minority fixed in *C. intestinalis*. They likely have originated from past admixture
193 events between the two species and then progressively been chopped down by recombination over
194 time while they drifted towards loss or fixation. The introgression hotspot on chromosome 5
195 immediately appears as an outlier on the chromosome map (**Figure 2**). Its underlying tracts were much
196 longer (maximal size of 156 Kb) than the tracts outside of the hotspot, and they segregated at
197 intermediate frequencies (none of the long tracts on the hotspot was fixed), in line with a recent
198 introgression event.

199 We then analyzed the coding sequences inside and outside the genomic tracts identified as
200 being introgressed (**Figure S3**). Chromosome 5 carries by far the largest number of introgressed CDS:
201 65 of 69 were located on this chromosome, while the four other introgressed CDS were located on
202 three different chromosomes (3, 8 and 13). Among all CDS on chromosome 5, 6% were detected as
203 being on introgressed tracts, demonstrating that the hotspot does contain introgressed genes. As
204 introgression has not reached fixation in *C. intestinalis*, we would expect an increase of diversity
205 within *C. intestinalis* (π) and a decrease of interspecies divergence (d_{XY}) for the CDS on introgressed
206 tracts compared to the rest of the genome. However, this is not what was observed (**Figure S3A**),
207 probably because the *C. robusta* introgressed alleles segregate at an intermediate frequency that
208 negligibly impacts diversity. Therefore, we computed the G_{\min} statistic, defined as the ratio of the
209 minimum d_{XY} to the average d_{XY} , which is better suited to capture the effect of recent introgression
210 events (Geneva et al. 2015). As expected if introgressed tracts originate from recent introgression

211 events, we found that G_{\min} was significantly lower in the introgressed CDS than in the rest of the
212 genome (**Figure S3B**).

213 The history of divergence and gene flow between *C. robusta* and *C. intestinalis*

214 In order to address whether short and long *C. robusta* tracts introgressed in the *C. intestinalis* genomes
215 could result from different introgression events, we reconstructed the divergence history between the
216 two species based on their joint site frequency spectrum. Divergence models in which the history of
217 gene flow can take different forms were tested. The possibilities of having a heterogeneity of effective
218 population sizes and effective migration rates to model the effects of linked selection and species
219 barriers were also included in the models. This is because previous work showed that when these
220 features were not considered, the inferences led to ambiguous results in sea squirts (Roux et al. 2016).
221 We first excluded chromosome 5 from the inferences to capture the prominent history between the two
222 species (**Figure 3** and **Table S3** for details). Divergence with periodic connectivity and the effects of
223 linked selection was the best model, closely followed by a secondary contact model. The divergence
224 between the two species started with gene flow (during ~400 Ky), then it was followed by a ~1.5 My
225 period of isolation. Only in the 30,000 last years, *C. robusta*, or a related lineage, and *C. intestinalis*
226 came into secondary contact. This long period of introgression could explain the presence of the short
227 introgressed tracts in *C. intestinalis*. In line with this scenario, the estimates of migration rates show
228 that introgression is highly asymmetrical from *C. robusta* toward *C. intestinalis*. Furthermore, we
229 observed a ten-fold lower effective population size in *C. robusta* than *C. intestinalis*, which matches
230 the difference in nucleotide diversities between the two species and can be explained by the recent
231 introduction of *C. robusta* in Europe (**Figure S1**). Repeating the demographic analyses with
232 chromosome 5 in the dataset led to very similar parameter estimates, except for the divergence times
233 (**Figure S5** and **Table S4** for details). Indeed, the best model was now a secondary contact, where a
234 long period of isolation (~2 My) was followed by a contemporary period of introgression (in the last
235 200 years), which may capture the signal left by the long introgressed tracts on chromosome 5.

236 We used a neutral recombination clock to refine the time estimate since admixture at the
237 introgression hotspot on chromosome 5. The average length of the introgressed tracts can be estimated
238 using the formula $\bar{L} = [(1 - f) * r * (t - 1)]^{-1}$, where r is the local recombination rate (crossovers
239 per base pair per generation), f is the admixture proportion, and t is the time since the admixture event
240 in generations (Racimo et al. 2015). Given that the average length of introgressed tracts at the hotspot
241 is 19,898 bp, the mean frequency of introgression is 0.106, and the recombination rate is 3.82e-07
242 M/bp (Duret, pers. comm.), we found that the contemporary admixture between *C. robusta* and *C.*
243 *intestinalis* occurred about 75 years ago (assuming two generations per year; Bouchemousse et al.
244 2017). Note that this point estimate for the date of introgression has to be considered carefully as
245 several factors can produce uncertainty around it. For example, a rapid rise in frequency due to
246 selection at the hotspot can create longer tracts than expected under neutral models. Additionally, we
247 used the genome-wide recombination rate for r , while the local recombination could be lower around
248 the hotspot. Finally, some introgressed tracts could be a bit longer than measured due to small regions
249 lacking sufficient ancestry signal (**Figure S7**).

250 The introgression hotspot on chromosome 5

251 We have shown that maximal F_{ST} values between *C. robusta* and *C. intestinalis* form a valley at the
252 start of chromosome 5 (**Figure 4A**). This pattern is due to long *C. robusta* tracts segregating in the
253 sympatric populations of *C. intestinalis* (**Figure 4B**). The introgression tracts were variable in size.
254 They shared ancestral recombination breakpoints, clearly visible in the linkage disequilibrium (LD)
255 heatmap between pairs of diagnostic SNPs along chromosome 5 (**Figure 4D**). The hotspot region
256 between 700 Kb and 1.5 Mb exhibited stronger LD (r^2 median of 0.3) than the rest of chromosome 5
257 (r^2 median of 0.007). Introgression was maximal on either side of the “missing data region” from
258 1,009,000 to 1,055,000 bp (a region of significantly increased read depth: 100x in average inside the
259 region vs 25x outside). But we found no evidence of introgressed tracts in the hotspot that have
260 completely swept to fixation in *C. intestinalis* (**Figure 4C**).

261 To explicitly test if some sort of selection could explain this pattern on chromosome 5, we
262 used various methods. We first sought the footprint of a classic selective sweep, where a *de novo*
263 beneficial mutation arises on a *C. robusta* haplotype and quickly sweeps toward fixation, reducing
264 diversity and creating a signal of long-range LD around it. This signal can be captured by the extended
265 haplotype homozygosity (EHH), which measures the decay of identity-by-descent between haplotypes
266 as a function of the distance from a focal SNP. Taking as targets the SNPs with the highest *C. robusta*
267 frequency to the left and right of the “missing data region”, we observed a slower EHH decay on the
268 *C. robusta* haplotypes compared to other haplotypes in the sympatric *C. intestinalis* populations, but
269 not in the *C. roulei* population (**Figure 4E**). To test for significance, the absolute normalized integrated
270 haplotype score (iHS) was then calculated in 50-Kb windows along chromosome 5, and we estimated
271 the proportion of SNPs in each window associated with outlying values of iHS. This proportion was
272 the highest in the core region of the introgression hotspot in *C. intestinalis* (8%) and *C. robusta* (20%),
273 but not in *C. roulei* (0%). This result indicates a low haplotype diversity over an extended region in
274 both the donor *C. robusta* and the introgressed alleles of the recipient *C. intestinalis* populations. The
275 genealogies of the 50-kb windows framing the “missing data region” further support a reduced
276 diversity of the *C. robusta* clade (**Figures 4F** and **S8**). Moreover, the alleles sampled in the
277 introgressed *C. intestinalis* genomes cluster within the star-like *C. robusta* clade, suggesting that a
278 recent selective sweep happened in *C. robusta* and a single beneficial haplotype introgressed into *C.*
279 *intestinalis*.

280 Finally, we used a complementary approach (VolcanoFinder) to directly test for adaptive
281 introgression using all SNPs from the *C. intestinalis* recipient species only. Again, the method is
282 suitable to detect an adaptively introgressed allele that has swept to fixation in the recipient species,
283 producing intermediate-frequency polymorphism in its flanking regions. Although introgression was
284 incomplete in our case (generating a soft sweep pattern, which may lead to a decrease in power), we
285 nonetheless observed a signal of adaptive introgression on the hotspot of chromosome 5 (**Figure S6B**).
286 Several other regions in the genome showed extreme values of the log-likelihood ratio test (**Figure**
287 **S6A**). However, contrary to the introgression hotspot, these regions also displayed signals of *de novo*

288 selective sweeps within *C. intestinalis* (detected with SweepFinder) that globally correlated with
289 genomic regions of reduced diversity (**Figure S1**). In contrast, a signal of *de novo* selective sweep
290 within *C. robusta* was detected in the introgression hotspot (**Figure S6B**), supporting the view that
291 beneficial alleles in this species recently swept to fixation and were adaptively introgressed into the
292 sympatric *C. intestinalis*.

293 Copy number variation at the introgression hotspot

294 We then annotated the introgression hotspot region of chromosome 5 (700 Kb - 1.5 Mb) to identify
295 putative candidate genes under selection. To overcome the difficulty posed by the high coverage of the
296 “missing data region” at the center of the hotspot, we relied on the variant allele fraction (VAF)
297 calculated from read depth to find candidate SNPs. Because the reference genome used throughout this
298 paper is from *C. robusta*, the variant allele represents the alternate allele in the *C. robusta* genome.
299 Candidate SNPs were defined as being differentiated between *C. robusta* and *C. roulei*, therefore
300 having a low VAF in the former and a high VAF in the latter, and being exclusively introgressed in the
301 sympatric *C. intestinalis* (VAF below 50%). Using a lenient threshold of VAF higher than 85% in *C.*
302 *roulei* and below 15% in *C. robusta*, we found 28 candidate SNPs in the 800-Kb region of the hotspot
303 distributed across six different protein-coding genes and two non-coding loci (**Figure S9**). Only
304 variants in the “missing data region” (20 of 28 SNPs) showed a coverage pattern in line with multi-
305 copy genes. Notably, 16 of these SNPs were located on the cytochrome P450 family 2 subfamily U
306 gene. Three other cytochromes from family 2 were found in the “missing data region” (subfamilies J/
307 D/R; **Figure S10**), but none contained candidate SNPs.

308 We did not find candidate SNPs where the *C. robusta* allele had swept to fixation in *C.*
309 *intestinalis*. The SNP showing the highest introgression frequency (0.85, i.e. only two non-
310 introgressed *C. intestinalis* individuals out of 13 sampled) was located in a single-copy non-coding
311 locus at position 1,067,404 bp. Nevertheless, this pattern should be interpreted with caution as many
312 individuals had a shallow read depth at this SNP. Considering the multi-copy genes, the 16 variants on
313 the cytochrome P450 all exhibited the same pattern of a high copy number of the introgressed *C.*

314 *robusta* allele, while this was not the case of the other multi-copy genes (**Figure S9**). Two candidate
315 SNPs on the cytochrome P450 are represented in **Figure 5**. They showed that *C. robusta* individuals
316 carried from five to twenty copies of the reference allele, while *C. roulei* individuals had one or two
317 copies of the alternate allele. As for the introgressed *C. intestinalis*, they were heterozygous with one
318 copy of the *C. intestinalis* allele and at least ten copies of the *C. robusta* allele, while the non-
319 introgressed *C. intestinalis* individuals were like *C. roulei*. This pattern suggests the presence of
320 multiple copies in tandem repeats of the *C. robusta* allele on cytochrome P450, which might play a
321 critical role in adaptation, and have favored its introgression into *C. intestinalis*.

322 Discussion

323 We used phased genomes from whole-genome trio sequencing to document the fine-scale genomic
324 consequences of the human-mediated contact between the invasive *C. robusta* and the native *C.*
325 *intestinalis* sea squirt species in Europe. A Mediterranean *C. roulei* population was also whole-genome
326 sequenced to be used as a non-introgressed control. Despite their high divergence, we have
327 demonstrated that the introduced and native species still hybridize in their sympatric range, showing a
328 localized introgression hotspot in the native species. We provided several lines of evidence for a sweep
329 of a selected allele in *C. robusta* that adaptively introgressed into *C. intestinalis* at the hotspot and
330 identified a tandem repeat variation at the cytochrome P450 locus to be a promising candidate.

331 Introgression between highly divergent sea squirt genomes

332 Introgression between highly divergent lineages has been rarely reported, partly because there is a bias
333 against studying the end of the speciation continuum (Kulmuni et al. 2020). Indeed, the few cases that
334 documented introgression between divergent species consistently showed that it was rare and localized
335 to small genomic regions, suggesting that most introgression events were deleterious in the recipient
336 genome. Moreover, introgression occurred more often in regions depleted in conserved elements and
337 regions with high recombination rates, consistent with the idea that introgressed tracts escape the
338 effect of species barriers through recombination (Martin and Jiggins 2017). Examples include

339 drosophila flies (Turissini and Matute 2017), coccidioides fungi (Maxwell et al. 2019), nine-spined
340 sticklebacks (Yamasaki et al. 2020), sea snails (Stankowski et al. 2020) or aspen trees (Shang et al.
341 2020).

342 In line with these previous studies, we observed limited introgression between the two
343 divergent sea squirt species in the sympatric range. We tested whether the presence of many short and
344 a few very long *C. robusta* introgressed tracts in the genome of the sympatric *C. intestinalis* species
345 could be explained by a complex history of gene flow between the two species. Therefore, we fitted
346 models that could include genomic heterogeneities in effective population sizes and migration rates as
347 well as periodic connectivity between the two species. Despite a firm species boundary with about
348 two-thirds of the genome linked to species barriers, we found signals of past introgression (in the last
349 ~30 Ky), far preceding their contemporary contact in Europe. This is in line with the low rates of
350 natural hybridization between the two species (Bouchemousse et al. 2016c). The past introgression
351 between *C. robusta* and *C. intestinalis* is puzzling given natural transoceanic migration was impossible
352 during glacial periods. The signal of introgression we detected might come from a ghost (extinct or
353 unsampled) lineage (Tricou et al. 2022) related to *C. robusta* that colonized the Atlantic at the
354 previous interglacial and came into contact with *C. intestinalis* during the last glacial maximum.
355 Indeed cryptic lineages are often found in the genus *Ciona* (Zhan et al. 2010; Mastrototaro et al. 2020)
356 that may prove better candidates for a 30 Ky old introgression event. The pattern of high
357 differentiation we observed along the genomes also suggests highly polygenic barriers that maintain
358 the species boundaries between *C. intestinalis* and *C. robusta* (or its relatives). As species diverged for
359 ~1.5 to 2 million years in strict isolation, they had time to accumulate many barriers in their genomes,
360 contributing to selection against introgression upon secondary contact.

361 These inferences were made excluding chromosome 5 to capture the prominent history
362 between the two species. When including this chromosome, and so the long introgressed tracts in the
363 introgression hotspot, we found evidence for a much more recent introgression event dated 200 years
364 ago. This estimate was then refined using a recombination clock and the introgressed tract length
365 distribution. We found that the contemporary introgression event may have occurred about 75 years

366 ago, consistent, this time, with the human-induced introduction of *C. robusta* in the English Channel
367 (Bouchemousse et al. 2016a; Nydam and Harrison 2011).

368 Is there an adaptive breakthrough on chromosome 5?

369 On top of the many short introgressed tracts (average length of 2.6 Kb) widespread in the *C.*
370 *intestinalis* genome and mostly segregating at a low frequency, we observed a very localized
371 introgression signal between 700 Kb and 1.5 Mb on chromosome 5. This hotspot of introgression
372 harbored very long introgression tracts (maximal length of 156 Kb) that were more frequent than the
373 baseline introgression level. This pattern contrasts with the tract length distribution observed in a
374 secondary contact between two divergent *Drosophila* fly species that diverged 3 My ago (Turissini and
375 Matute 2017). Introgression produced mostly small tracts (1 to 2.5 Kb on average), but the longest
376 tracts were only 7.5 to 10 Kb long, ten times smaller than what was observed in the sea squirt hotspot.
377 The situation in sea squirts resembles more to the introgression pattern between two fungi species that
378 diverged 5 My ago (Maxwell et al. 2019). Most introgression tracts were 3 to 4 Kb long on average
379 and segregated at low frequency, but there was a long tail of longer tracts (maximal length of 100 Kb),
380 some of them being found in high frequency within species.

381 Adaptive introgressed alleles are expected to increase in frequency in the recipient population.
382 However, alleles might also increase in frequency simply due to allele surfing at the front wave of a
383 range expansion (Klopfstein et al. 2006). In our study, we only sampled populations in the English
384 Channel (Aber and Brest), but Le Moan et al. (2021) demonstrated that the introgression hotspot was
385 present in multiple localities (10 of 18) across the contact zone (Bay of Biscay, Iroise Sea and the
386 English Channel). The populations we sampled in Aber and Brest were among the most introgressed,
387 together with populations in the western UK coastline. However, there was no evidence for a wave of
388 introgression in line with geography: the distribution of introgressed tracts was a geographic mosaic,
389 likely due to human-mediated transportation (Le Moan et al. 2021).

390 Furthermore, the introgression of genomic tracts across a species barrier is highly random at
391 short time scales. Therefore, one expects a large variance in the tract length distribution under neutral

392 admixture (Sachdeva and Barton 2018). Observing long haplotypes at intermediate frequency could
393 thus be explained with purely neutral processes, especially if the hotspot corresponds to a region of
394 reduced recombination (duplicated repeats may be an underestimated way to arrest recombination
395 locally in the genomes, e.g., Kim et al. 2022). Still, the singularity of such a region found in the
396 genome of sympatric *C. intestinalis* individuals seems difficult to explain without invoking some sort
397 of selection. We identified signals of selection based on haplotype variations in the flanking regions of
398 the most introgressed alleles (Sabeti et al. 2002; Staubach et al. 2012). Indeed, the introgression
399 hotspot is characterized by unusually long-range LD in the introgressed *C. intestinalis* population. The
400 genealogy at the hotspot shows that the haplotypes sampled in *C. intestinalis* cluster together with the
401 start-like clade of the *C. robusta* haplotypes. This indicates that a recent selective sweep occurred in
402 the *C. robusta* population, leading to the fixation of a beneficial allele, which then introgressed into the
403 sympatric *C. intestinalis* populations. This scenario was supported using an independent method based
404 on polarized SNPs (Setter et al. 2020; Szpiech et al. 2021).

405 Nevertheless, we cannot claim yet that the hotspot on chromosome 5 contains alleles that were
406 adaptively introgressed *sensu stricto*. Indeed, the introgression is not fixed in the studied *C.*
407 *intestinalis* population (maximal frequency of 0.31), nor in other distant localities of the contact zone
408 included in Le Moan et al. (2021). Le Moan et al. (2021) suggested that the maintenance of
409 polymorphism at these alleles could be explained with some sort of balancing selection: if the
410 introgressed tracts are under overdominance or frequency-dependent selection, and suffer a fitness
411 reduction when frequent and homozygous in a foreign genetic background. Therefore, an incomplete
412 sweep aligns with balancing selection acting on the introgressed alleles (e.g., humans and
413 neanderthals: Sams et al. 2016). In addition, this pattern is also expected if admixture is very recent,
414 typically when it has been human-mediated, as then allele replacement may still be ongoing in the
415 recipient population. For example, this may be the case in honeybees where a haplotype of European
416 ancestry, implicated in reproductive traits and foraging, was found at high frequency, but not fixed, in
417 Africanized honeybees (Nelson et al. 2017), confirmed in Calfee et al. (2020). Incomplete
418 introgression at a single region has also been documented in cotton bollworm, where an insecticide

419 resistance allele at a cytochrome P450 gene increased in frequency after introducing an invasive
420 congener carrying the adaptation (Valencia-Montoya et al. 2020).

421 A usual suspect: cytochrome P450

422 In the middle of the introgression hotspot, we identified a region with high coverage that we could not
423 analyze using called genotypes (from 1,009,000 to 1,055,000 bp). Therefore, we examined the read
424 depth at candidate SNPs in this genomic region to identify further variants introgressing at a high
425 frequency. This analysis pinpointed 28 candidate SNPs, of which one in a non-coding region was at a
426 high frequency (0.85), but its overall low read depth calls for caution. The second most introgressed
427 SNPs ($n=16$) were located on the cytochrome P450 family 2 subfamily U gene, and all showed the
428 same introgression pattern with a frequency of 0.35. Strikingly, the *C. robusta* alleles had a read depth
429 pattern consistent with them being multi-copy (5 to 20 copies), while this was not the case for the *C.*
430 *intestinalis* alleles sampled in the non-introgressed individuals.

431 These candidate variants could potentially be involved in adaptation. Notably, the cytochrome
432 P450 gene is an exciting candidate. It belongs to a large gene class of oxidase enzymes responsible for
433 the biotransformation of small endogenous molecules, detoxifying exogenous compounds, and it is
434 involved in regulating the circadian rhythm. Cytochrome P450 family 2 is the largest and most diverse
435 CYP family in vertebrates, and the U and R subfamilies were present in the vertebrate ancestor
436 (Nelson 1998). A recent study experimentally showed that the candidate gene we identified here
437 (cytochrome P450 2U) is involved in the inflammatory response in *C. robusta* (Vizzini et al. 2021).
438 Although this phenotype indicates resistance toward toxic substances, future functional study of
439 potential fitness differences between the tandem repeat *C. robusta* allele and the single copy *C.*
440 *intestinalis* allele will be needed to determine what adaptive role these alleles play. Note, however, that
441 if the tandem-repeat variant provides adaptation to pollution in harbors, this would result in local
442 selection and explain the absence of fixation (the native alleles being fitter in wild habitats), as
443 discussed above.

444 At a larger phylogenetic scale, resistance genes were identified as gene families enriched in
445 adaptive introgressions (Moran et al. 2021). Notably, human-induced selection such as insecticide
446 exposure drives strong and rapid development of resistance. In that context, gene amplification of
447 detoxification enzymes is a crucial feature for adaptation as it increases the number of functional
448 enzymes and/or allows neofunctionalization of the new copies. There are many examples of such
449 processes involving cytochromes P450 in insects. Insecticide resistance is due to gene amplification
450 that produces over-expression of the cytochrome P450 gene in the aphid *Myzus persicae*
451 (neonicotinoids resistance, Puinean et al. 2010), *Drosophila melanogaster* (DDT resistance, Schmidt
452 et al. 2010), *Anopheles funestus* (pyrethroid resistance, Wondji et al. 2009), and *Anopheles coluzzii*
453 (ITN resistance, Main et al. 2018). Neonicotinoids resistance due to neofunctionalization of a
454 duplicated cytochrome P450 was demonstrated in the brown planthopper, *Nilaparvata lugens* (Zimmer
455 et al. 2018). Another example of high copy numbers of cytochrome P450 conferring insecticide
456 resistance was found in the moth *Spodoptera frugiperda* (Yainna et al. 2021). In contrast, resistance
457 against pyrethroid in the moth *Helicoverpa armigera* and introgressed *Helicoverpa zea* was due to a
458 chimeric cytochrome P450 gene resulting from recombination between two copies in tandem
459 (Valencia-Montoya et al. 2020).

460 Even though we are not yet at the step of functionally characterizing the cytochrome P450
461 candidate gene, we highlighted in this work the critical role of biological invasions for driving
462 adaptive introgression across species boundaries. Our work also illustrates that phased genomes offer
463 the opportunity to detect introgression signals between divergent species, even when they are rare and
464 localized in the genome. Genomically localized introgression breakthroughs are still an understudied
465 pattern that recent genomic surveys have only begun to unravel.

466 Materials and Methods

467 Sampling and whole-genome sequencing

468 Sixteen parent-offspring trios (six interspecific, six within *Ciona intestinalis* and four within *Ciona*
469 *robusta*) were generated by crossing wild-caught parents in the laboratory at Roscoff (**Table S1**).

470 Species were identified first by using morphological criteria (Sato et al. 2012; Brunetti et al. 2015).
471 Morphological species identification was further validated using a diagnostic mitochondrial locus
472 (mtCOI, following Nydam and Harrison 2007). For *C. intestinalis*, seven of the parents used were
473 sampled in the marina of the Aber Wrac'h (Finistère, France), and nine others in the marina of Moulin
474 Blanc, Brest (Finistère, France). For *C. robusta*, the ten parents used were also sampled in Moulin
475 Blanc. The two parents and one randomly selected descendant for each trio were fixed in absolute
476 ethanol, and their whole genomic DNA was extracted using a CTAB protocol. Five individuals were
477 sampled in Banyuls-Sur-Mer (Méditerranée, France) belonging to *Ciona roulei*. Based on crossing
478 experiments and genetic analyses, the species status of *C. roulei* has been repeatedly questioned
479 (Nydam and Harrison 2010; Malfant et al. 2018; Le Moan et al. 2021). In particular, recent genetic
480 analyses clearly showed that *C. roulei* is a distinct lineage of *C. intestinalis*, specific to the
481 Mediterranean Sea (Le Moan et al. 2021). Therefore, we used these individuals as a positive control
482 for a non-introgressed population of *C. intestinalis*. For *C. roulei* samples, genomic DNA was
483 extracted using a Nucleospin Tissue kit (Macherey-Nagel). After quality control, DNA extracts were
484 sent to the LIGAN genomics platform (Lille, France) where whole-genome sequencing libraries were
485 prepared separately for each of the 48 individuals, and were sequenced on an Illumina Hi-Seq 2000
486 instrument using 100 bp PE reads. Three poorly sequenced parents (ad2, ad18 and ad31; **Table S1**)
487 were excluded from analyses.

488 Furthermore, four *Ciona edwardsi* individuals were sampled in Banyuls-Sur-Mer. *C. edwardsi*
489 is reproductively isolated from the other taxa included in this study, and it was used as an outgroup
490 (Malfant et al. 2018). These individuals were fixed in RNAlater, and their DNA was extracted using a
491 Nucleospin Tissue kit (Macherey-Nagel). Libraries were prepared separately for each of the four
492 individuals, and were sequenced on an Illumina Hi-Seq 4000 instrument using 150 bp PE reads at
493 FASTERIS (Plan-les-Ouates, Switzerland).

494 Genotyping and haplotyping pipeline

495 We followed the GATK best practice pipeline (Van der Auwera et al. 2013) including haplotype
496 phasing-by-transmission, as applied in Duranton et al. (2018). All scripts used in the pipeline are
497 available in the **Supplementary Scripts**. We generated seven different datasets with various levels of
498 filtering, and with or without haplome phasing, that are described in the **Supplementary Data** (see
499 **Table S5** for details).

500 All analyses were made using the newly available *C. robusta* assembly as the reference
501 genome (GCA_009617815.1; Satou et al. 2019). As a cautionary note, analyses in Le Moan et al.
502 (2021) were made using the previous *C. robusta* reference genome published in 2011
503 (GCA_000224145.1), therefore coordinates do not correspond between the two studies. After quality
504 control with FastQC v0.11.2, reads were aligned to the *C. robusta* reference genome using BWA-mem
505 v0.7.5a (Li and Durbin 2009), and duplicates were marked using Picard v1.119. The individual bam
506 files of the introgression hotspot were used as dataset #7. The mean read depth was 21x across all
507 samples (**Table S1**).

508 A series of steps were then performed using GATK v3.4-0 (McKenna et al. 2010), including:
509 *i*) local realignment around indels, *ii*) individual variant calling in gVCF format using the
510 HaplotypeCaller (options: dontUseSoftClippedBases, heterozygosity=0.01, minimum base quality
511 score=30), *iii*) joint genotyping using GenotypeGVCFs (heterozygosity=0.01), *iv*) genotype
512 refinement based on family priors. Hard-filtering was then applied on the SNPs and indels to produce
513 a database of high-confidence variants. The database was then used to recalibrate variant quality
514 scores with the VQSR algorithm. After recalibration, a second round of genotype refinement based on
515 family priors was applied.

516 We then introduced a step of genotype verification (and correction where required) to check
517 for reference bias and miscalling. First, we computed the individual variant allele fraction (VAF) at
518 each site, i.e. the ratio of the alternate allele depth to the total (alternate+reference) depth. Then, a
519 distribution across sites was plotted for the three possible genotypes (homozygous reference: 0/0,
520 heterozygous: 0/1, homozygous alternate: 1/1). While the distributions for the homozygous genotypes
521 were shaped as expected (i.e. 99% of the sites had a VAF < 0.1 for 0/0 and VAF > 0.9 for 1/1), the

522 distribution of heterozygous genotypes was normally distributed around VAF=0.5, but showed
523 additional peaks near 0 (and near 1 to a lesser extent). Therefore, we corrected the miscalled 0/1
524 genotypes to 0/0 when the variant allele depth was below the 99th quantile of the 0/0 distribution and
525 to 1/1 when it was above the 1th quantile of the 1/1 distribution. In addition, heterozygous genotypes
526 with a VAF $< \frac{1}{3}$ or $> \frac{2}{3}$ were assigned as missing data (excluding the ones we corrected near VAF=0 or
527 1). We also considered as missing data the genotypes with a total depth below ten reads or above the
528 99th quantile of the depth distribution (to exclude repeated regions). Finally, low-quality variants were
529 excluded from the VCF (QUAL<30), and we applied a stringent filter on individual genotype quality
530 (GQ<30). Different missing data thresholds were then applied to produce datasets #2 (five missing
531 genotypes), #5 (no missing genotypes allowed) and #6 (three missing genotypes).

532 Phased genomes were obtained using the tool PhaseByTransmission of GATK v3.4-0. All trios
533 were phased given parents and offspring genotype likelihoods, setting a *de novo* mutation prior to $1e-8$
534 /bp/year (estimated for sea squirts in Tsagkogeorga et al. 2012). Only sites where Mendelian
535 transmission could be determined unambiguously were phased. The non-missing phased SNPs were
536 then used as a reference panel for BEAGLE v4.0 (Browning and Browning 2007). BEAGLE was run
537 without imputing genotypes (impute=false) on the filtered VCF, with all variants being unphased. The
538 parent-offspring relationships in the reference panel were specified to inform phasing-by-transmission
539 with BEAGLE, except for the five *C. roulei* samples, which were not included in a trio and were
540 statistically phased. Datasets #1, #3 and #4 are based on this phased VCF.

541 A genomic region with high coverage failed to be genotyped in the introgression hotspot
542 (defined between 700 Kb and 1.5 Mb). This region was set as the “missing data region” and defined
543 from 1,009,000 to 1,055,000 bp.

544 Analyses of population structure

545 We used a Principal Component Analysis (PCA) to assess the partition of genetic variation in our
546 sample of 45 individuals (i.e. all individuals except the three poorly sequenced parents, and the *C.*
547 *edwardsi* individuals). SNPs were LD-pruned with PLINK v1.9 (Purcell et al. 2007) using a window

548 size (WD) of 20 SNPs, a window step size (CT) of 5 SNPs and a linkage threshold (r^2) of 0.1. PLINK
549 was then used to run a PCA on the unlinked SNPs. We recorded the amount of genotypic variance
550 explained by each principal component (PC) and the SNP weights on each PC. Only the first two PCs
551 were relevant to visualize population structure and were plotted using the R package tidyverse.

552 We used VCFtools v0.1.15 (Danecek et al. 2011) on all SNPs to calculate the per-site
553 nucleotide diversity (site- π) in each population and the per-site F_{ST} (weir-fst-pop, Weir and
554 Cockerham 1984) between populations. We then calculated the average and maximum of these
555 statistics for each chromosome in non-overlapping windows of 10 Kb. Windows with less than 10
556 SNPs were excluded. The linkage disequilibrium on chromosome 5 (where an introgression hotspot
557 was detected) in the *C. intestinalis* individuals was estimated with the function “hap-r2” of VCFtools.
558 It was based on the calculation of the r^2 among all fixed SNPs (phased) between *C. robusta* and *C.*
559 *roulei*.

560 Detection of introgression with summary statistics

561 To evaluate the extent of genome-wide admixture, we computed the D-statistic (Green et al. 2010;
562 Patterson et al. 2012) from a polarized set of SNPs using the outgroup species, *C. edwardsi*. The
563 following topology was applied: (((P1 = *C. roulei* ; P2 = *C. intestinalis*) ; P3 = *C. robusta*) ; O = *C.*
564 *edwardsi*). Therefore, a positive value of D indicates an excess of ABBA sites, and so an excess of
565 shared ancestry of *C. robusta* with *C. intestinalis* over that shared with *C. roulei*. We also estimated the
566 fraction of the genome introgressed with the *fd* statistic (Martin et al. 2015), calculated in non-
567 overlapping windows of 100 SNPs. The D and *fd* statistics were computed following Simon Martin's
568 tutorial: https://github.com/simonhmartin/tutorials/blob/master/ABBA_BABA_whole_genome/README.md

569 Detection of introgression with local ancestry inference

570 We used Chrompainter (available in fineSTRUCTURE v2.0.7) to perform local ancestry inference
571 based on the phased dataset. *C. intestinalis* was considered as the recipient population, while *C.*
572 *robusta* and *C. roulei* (the latter being a non-introgressed population of *C. intestinalis*) were the donor
573 populations. We used ten iterations of the expectation-maximization algorithm to estimate the
574 probability of each position along each *C. intestinalis* haplotype to come from *C. robusta* or *C. roulei*.
575 We then determined the boundaries of each ancestry tract. A given position was considered originating
576 from *C. robusta* if this probability was >0.95. To define the tracts, an extension from this focal position
577 was then made as long as this probability was above 0.5 at the surrounding positions (Duranton et al.
578 2018).

579 Various statistics were then calculated focusing on the introgressed tracts originating from *C.*
580 *robusta* (i.e. those found in *C. intestinalis* haplotypes, but with a *C. robusta* ancestry): *i*) the *C. robusta*
581 ancestry fraction per individual, *ii*) the tract length, and *iii*) the frequency of the alleles lying on the
582 tracts. No filter on the minimal tract length was applied, and missing data were not allowed for the
583 allele frequency calculation.

584 We performed additional analyses on the coding sequences (CDS). They were obtained by
585 extracting the biallelic SNPs from the phased VCF. Then, the VCF was converted into a fasta file, and
586 exons were extracted with bedtools v2.25.0 based on the annotation file (HT.Gene.gff3) of the
587 reference genome. The CDS were classified as introgressed or not using the bounds inferred from
588 Chromopainter. The following statistics were calculated for the CDS: *i*) the pairwise nucleotide
589 diversity (π , Tajima 1983), *ii*) the raw divergence between *C. robusta* and *C. intestinalis* (d_{XY} , Nei and
590 Li 1979), and *iii*) the G_{\min} measured as $\text{minimum}(d_{XY})/\text{average}(d_{XY})$ (Geneva et al. 2015).

591 Testing for selection

592 Selection for an adaptive variant is expected to reduce haplotype variation in flanking regions,
593 producing unusually long haplotypes (Sabeti et al. 2002). To capture such a signal, we measured the
594 extended haplotype homozygosity (EHH) score from the phased dataset using SelScan v2.0.0 (Szpiech
595 2021). Target SNPs were identified as the *C. robusta* alleles with the highest frequency to the left
596 (959,519 bp) and right (1,061,854 bp) of the “missing data region” on chromosome 5. The maximum
597 extension from the target SNP for a single EHH computation was 100 Kb. Then, we calculated with
598 SelScan the (absolute) integrated haplotype score (iHS). Values were normalized using the norm
599 v1.3.0 utility with 100 frequency bins over 50-Kb non-overlapping windows. Finally, we estimated the
600 proportion of SNPs in each window associated with extreme iHS values ($iHS > 3$, which refers to the
601 99th quantile of the iHS distribution).

602 We also tested for the footprint of selective sweeps using SweepFinder v2.0 (DeGiorgio et al.
603 2016) and adaptive introgression using VolcanoFinder v1.0 (Setter et al. 2020). These methods are
604 based on polarized SNPs (using the outgroup species *C. edwardsi*) and do not use phase information.
605 Chromosomes were scanned with the two methods applying a log-ratio test for selection at test sites
606 spaced by 1Kb.

607 Finally, SplitsTree4 V4.17.0 (Huson and Bryant 2006) was used on the phased dataset to
608 produce neighbor-joining trees from 50-Kb windows framing the “missing data region” on
609 chromosome 5.

610 Analyses of copy number variation

611 To overcome the absence of genotyping in the “missing data region” (due to our filtering of repeated
612 regions), we analyzed the read depth of the variants directly from the unfiltered bam files. Counts of
613 the reference and alternate alleles were collected with GATK (CollectAllelicCounts) from the bam
614 files, excluding duplicate reads and positions with a base quality (BQ) < 20. Candidate SNPs were
615 defined based on their variant allele fraction (VAF = alternate read depth / total read depth). The
616 following criteria were applied to identify variants differentiated between *C. robusta* and *C. roulei* (the
617 latter is used as a non-introgressed *C. intestinalis* population), and introgressed into *C. intestinalis*:
618 VAF <= 50% in *C. intestinalis*, VAF >= 85% (or 90%) in *C. roulei* and VAF <= 15% (or 10%) in *C.*
619 *robusta*. The copy number at each candidate SNP was then calculated as its allele read depth
620 normalized by the per-site read depth averaged across all sites (excluding sites with less than ten
621 reads) for each individual. Variants were annotated using the HT.Gene.gff3 file of the reference
622 genome.

623 Demographic inferences

624 We reconstructed the divergence history of *C. robusta* and *C. intestinalis* from the folded joint site
625 frequency spectrum (jSFS) using moments (Jouganous et al. 2017). No missing data was allowed, and
626 the SNPs were LD-pruned with PLINK v1.9 using a window size (WD) of 10 SNPs, a window step
627 size (CT) of 10 SNPs and a linkage threshold (r^2) of 0.5. We defined five demographic scenarios,
628 following (Fraïsse et al. 2018): SI = strict isolation, IM = isolation with continuous migration, SC =
629 secondary contact, AM = ancient migration, PER = periodic connectivity with both an ancient and a
630 current period of gene flow. Different versions of these scenarios were tested, following (Fraïsse et al.
631 2021): bbN = genomic heterogeneity of the effective population sizes (to capture the effect of
632 background selection), bbM = genomic heterogeneity of the effective migration rates (to capture the
633 effect of interspecies barriers to gene flow), 2N2M = combining both types of heterogeneities, “” = no
634 heterogeneities. Parameters were as follows: T = times in years (assuming two generations per year in
635 European waters), N_e = effective population sizes in numbers of individuals, m = migration rates

636 (independently estimated in both directions), %Barriers = fraction of the genome experiencing null
637 migration (i.e. species barriers and their associated loci), %Ne_{reduced} = fraction of the genome
638 experiencing reduced Ne due to background selection, HRF = factor by which Ne is reduced. See
639 **Tables S3** and **S4** for details. The scripts used to define the demographic models and run the
640 inferences are available in the **Supplementary Scripts**.

641 Each demographic model was then fitted to the observed jSFS, with singletons masked. We
642 ran five independent runs from randomized starting parameter values for each model. Likelihood
643 optimization was performed using a “dual annealing” algorithm (optimize_dual_anneal). It consists of
644 a series of global optimizations, each followed by a local optimization (“L-BFGS-B” method).
645 Settings of the global optimizations were as follows: maximum number of search iterations = 100,
646 initial temperature = 50, acceptance parameter = 1, and visit parameter = 1.01. The maximum number
647 of search iterations for the local optimization was set to 100. Model comparisons were made using the
648 Akaike information criterion (AIC), calculated as $2*k - 2*ML$, where k is the number of parameters in
649 the model, and ML its maximum log-likelihood value across the five runs.

650 Data Availability

651 Sequence reads have been deposited in NCBI Sequence Read Archive (SRA) under the accession
652 number PRJNA813009. Supplementary Data is available from Zenodo: 10.5281/zenodo.6992403.
653 Supplementary Figures, Tables and Scripts can be found in the Supporting Information.

654 Funding

655 This work benefited from funding of the French National Research Agency (ANR) with regards the
656 ANR Project HYSEA (no. ANR-12-BSV7-0011). It also benefited from the MarEEE project funded
657 through the French National Research Agency (ANR) under the “Investissements d’Avenir”
658 programme with the reference ANR-16-IDEX-0006 (i-site MUSE). The funders had no role in study
659 design, data collection and analysis, decision to publish, or preparation of the manuscript.

660 Conflict of interest disclosure

661 The authors declare they have no conflict of interest relating to the content of this article. Nicolas
662 Bierne, Pierre-Alexandre Gagnaire and Christelle Fraïsse are recommenders for PCI.

663 Acknowledgments

664 The authors are grateful to the divers of the Marine Operations department (*Service Mer &*
665 *Observation*) at the Roscoff Biological Station for the *Ciona* sampling in Brittany, and to Marine
666 Malfant, Sebastien Darras and divers of the laboratory Arago in Banyuls-Sur-Mer for providing the
667 *Ciona edwardsi* and *C. roulei* samples, and Charlotte Roby for DNA extractions. The authors are very
668 thankful to Jerome Coudret and Sarah Bouchemousse for their help for carrying the laboratory crosses
669 at Roscoff. We thank Véronique Dhennin from the LIGAN genomics platform (Lille, France), and
670 Nicolas González from the FASTERIS platform (Plan-les-Ouates, Switzerland). This work benefited
671 from the Montpellier Bioinformatics Biodiversity platform supported by the LabEx CeMEB, an ANR
672 "Investissements d'avenir" program (ANR-10-LABX-04-01).

673 References

- 674 Bouchemousse S, Bishop JDD, Viard F. 2016a. Contrasting global genetic patterns in two biologically
675 similar, widespread and invasive *Ciona* species (Tunicata, Ascidiacea). *Sci. Rep.* 6:24875.
- 676 Bouchemousse S, Lévêque L, Dubois G, Viard F. 2016b. Co-occurrence and reproductive synchrony
677 do not ensure hybridization between an alien tunicate and its interfertile native congener. *Evol.*
678 *Ecol.* 30:69–87.
- 679 Bouchemousse S, Liautard-Haag C, Bierne N, Viard F. 2016c. Distinguishing contemporary
680 hybridization from past introgression with postgenomic ancestry-informative SNPs in strongly
681 differentiated *Ciona* species. *Mol. Ecol.* 25:5527–5542.
- 682 Bouchemousse S, Lévêque L, Viard F. 2017. Do settlement dynamics influence competitive

- 683 interactions between an alien tunicate and its native congener? *Ecol. Evol.* 7:200–213.
- 684 Browning SR, Browning BL. 2007. Rapid and accurate haplotype phasing and missing-data inference
685 for whole-genome association studies by use of localized haplotype clustering. *Am. J. Hum.*
686 *Genet.* 81:1084–1097.
- 687 Brunetti R, Gissi C, Pennati R, Caicci F, Gasparini F, Manni L. 2015. Morphological evidence that the
688 molecularly determined *Ciona intestinalis* type A and type B are different species: *Ciona robusta*
689 and *Ciona intestinalis*. *J. Zoolog. Syst. Evol. Res.* 53: 186–193.
- 690 Calfee E, Agra MN, Palacio MA, Ramírez SR, Coop G. 2020. Selection and hybridization shaped the
691 rapid spread of African honey bee ancestry in the Americas. *PLoS Genet.* 16:e1009038.
- 692 Danecek P, Auton A, Abecasis G, Albers CA, Banks E, DePristo MA, Handsaker RE, Lunter G, Marth
693 GT, Sherry ST, et al. 2011. The variant call format and VCFtools. *Bioinformatics* 27:2156–2158.
- 694 DeGiorgio M, Huber CD, Hubisz MJ, Hellmann I, Nielsen R. 2016. SweepFinder2: increased
695 sensitivity, robustness and flexibility. *Bioinformatics* 32:1895–1897.
- 696 Durantón M, Allal F, Fraïsse C, Bierne N, Bonhomme F, Gagnaire P-A. 2018. The origin and
697 remolding of genomic islands of differentiation in the European sea bass. *Nature Comm.* 9:2518.
- 698 Fraïsse C, Popovic I, Mazoyer C, Spataro B, Delmotte S, Romiguier J, Loire É, Simon A, Galtier N,
699 Duret L, et al. 2021. DILS: Demographic inferences with linked selection by using ABC. *Mol.*
700 *Ecol. Resour.* 21:2629–2644.
- 701 Fraïsse C, Roux C, Gagnaire P-A, Romiguier J, Faivre N, Welch JJ, Bierne N. 2018. The divergence
702 history of European blue mussel species reconstructed from Approximate Bayesian Computation:
703 the effects of sequencing techniques and sampling strategies. *PeerJ* 6:e5198.
- 704 Geneva AJ, Muirhead CA, Kingan SB, Garrigan D. 2015. A New Method to Scan Genomes for
705 Introgression in a Secondary Contact Model. *PLoS One* 10:e0118621.

- 706 Green RE, Krause J, Briggs AW, Maricic T, Stenzel U, Kircher M, Patterson N, Li H, Zhai W, Fritz
707 MH-Y, et al. 2010. A draft sequence of the Neandertal genome. *Science* 328:710–722.
- 708 Hudson J, Viard F, Roby C, Rius M. 2016. Anthropogenic transport of species across native ranges:
709 unpredictable genetic and evolutionary consequences. *Biol. Lett.* 12:20160620.
- 710 Huson DH, Bryant D. 2006. Application of phylogenetic networks in evolutionary studies. *Mol. Biol.*
711 *Evol.* 23:254–267.
- 712 Jouganous J, Long W, Ragsdale AP, Gravel S. 2017. Inferring the joint demographic history of
713 multiple populations: beyond the diffusion approximation. *Genetics* 206:1549–1567.
- 714 Kaback DB. 1996. Chromosome-size dependent control of meiotic recombination in humans. *Nat.*
715 *Genet.* 13:20–21.
- 716 Kim K-W, De-Kayne R, Gordon IJ, Saitoti Omufwoko K, Martins DJ, French-Constant RF, Martin
717 SH. 2022. Stepwise evolution of a butterfly supergene via duplication and inversion. *Philos.*
718 *Trans. R. Soc. Lond. B.* 377: 20210207.
- 719 Klopstein S, Currat M, Excoffier L. 2006. The fate of mutations surfing on the wave of a range
720 expansion. *Mol. Biol. Evol.* 23:482–490.
- 721 Kulmuni J, Butlin RK, Lucek K, Savolainen V, Westram AM. 2020. Towards the completion of
722 speciation: the evolution of reproductive isolation beyond the first barriers. *Philos. Trans. R. Soc.*
723 *Lond. B Biol. Sci.* 375:20190528.
- 724 Le Moan A, Roby C, Fraïsse C, Daguin-Thiébaud C, Bierne N, Viard F. 2021. An introgression
725 breakthrough left by an anthropogenic contact between two ascidians. *Mol. Ecol.* 30:6718–6732.
- 726 Li H, Durbin R. 2009. Fast and accurate short read alignment with Burrows-Wheeler transform.
727 *Bioinformatics* 25:1754–1760.

- 728 Main BJ, Everitt A, Cornel AJ, Hormozdiari F, Lanzaro GC. 2018. Genetic variation associated with
729 increased insecticide resistance in the malaria mosquito, *Anopheles coluzzii*. *Parasit. Vectors*
730 11:225.
- 731 Malfant M, Darras S, Viard F. 2018. Coupling molecular data and experimental crosses sheds light
732 about species delineation: a case study with the genus *Ciona*. *Sci. Rep.* 8:1480.
- 733 Martin SH, Davey JW, Jiggins CD. 2015. Evaluating the use of ABBA–BABA statistics to locate
734 introgressed loci. *Mol. Biol. Evol.* 32:244–257.
- 735 Martin SH, Jiggins CD. 2017. Interpreting the genomic landscape of introgression. *Curr. Opin. Genet.*
736 *Dev.* 47:69–74.
- 737 Mastrototaro F, Montesanto F, Salonna M, Viard F, Chimienti G, Trainito E, Gissi C. 2020. An
738 integrative taxonomic framework for the study of the genus *Ciona* (Ascidiacea) and description of
739 a new species, *Ciona intermedia*. *Zool. J. Linn. Soc.* 190:1193–1216.
- 740 Maxwell CS, Mattox K, Turissini DA, Teixeira MM, Barker BM, Matute DR. 2019. Gene exchange
741 between two divergent species of the fungal human pathogen, *Coccidioides*. *Evolution* 73:42–58.
- 742 McFarlane SE, Pemberton JM. 2019. Detecting the true extent of introgression during Anthropogenic
743 hybridization. *Trends Ecol. Evol.* 34:315–326.
- 744 McKenna A, Hanna M, Banks E, Sivachenko A, Cibulskis K, Kernytsky A, Garimella K, Altshuler D,
745 Gabriel S, Daly M, et al. 2010. The Genome Analysis Toolkit: a MapReduce framework for
746 analyzing next-generation DNA sequencing data. *Genome Res.* 20:1297–1303.
- 747 Moran BM, Payne C, Langdon Q, Powell DL, Brandvain Y, Schumer M. 2021. The genomic
748 consequences of hybridization. *Elife* 10:e69016.
- 749 Nei M, Li WH. 1979. Mathematical model for studying genetic variation in terms of restriction
750 endonucleases. *Proc. Natl. Acad. Sci. U. S. A.* 76:5269–5273.

- 751 Nelson DR. 1998. Metazoan cytochrome P450 evolution. *Comp. Biochem. Physiol. C Pharmacol.*
752 *Toxicol. Endocrinol.* 121:15–22.
- 753 Nelson RM, Wallberg A, Simões ZLP, Lawson DJ, Webster MT. 2017. Genomewide analysis of
754 admixture and adaptation in the Africanized honeybee. *Mol. Ecol.* 26:3603–3617.
- 755 Noé L, Kucherov G. 2005. YASS: enhancing the sensitivity of DNA similarity search. *Nucleic Acids*
756 *Res.* 33:W540–W543.
- 757 North HL, McGaughran A, Jiggins CD. 2021. Insights into invasive species from whole-genome
758 resequencing. *Mol. Ecol.* 30:6289–6308.
- 759 Nydam ML, Harrison RG. 2007. Genealogical relationships within and among shallow-water Ciona
760 species (Ascidiacea). *Mar. Biol.* 151: 1839–1847.
- 761 Nydam ML, Harrison RG. 2010. Polymorphism and divergence within the ascidian genus Ciona. *Mol.*
762 *Phylogenet. Evol.* 56:718–726.
- 763 Nydam ML, Harrison RG. 2011. Introgression despite substantial divergence in a broadcast spawning
764 marine invertebrate. *Evolution* 65:429–442.
- 765 Purcell S, Neale B, Todd-Brown K, Thomas L, Ferreira MAR, Bender D, Maller J, Sklar P, de Bakker
766 PIW, Daly MJ, Sham PC. 2007. PLINK: a toolset for whole-genome association and population-
767 based linkage analysis. *Am. J. Hum. Genet.* 81.
- 768 Ottenburghs J. 2021. The genic view of hybridization in the Anthropocene. *Evol. Appl.* 14:2342–2360.
- 769 Patterson N, Moorjani P, Luo Y, Mallick S, Rohland N, Zhan Y, Genschoreck T, Webster T, Reich D.
770 2012. Ancient admixture in human history. *Genetics* 192:1065–1093.
- 771 Puinean AM, Foster SP, Oliphant L, Denholm I, Field LM, Millar NS, Williamson MS, Bass C. 2010.
772 Amplification of a cytochrome P450 gene is associated with resistance to neonicotinoid

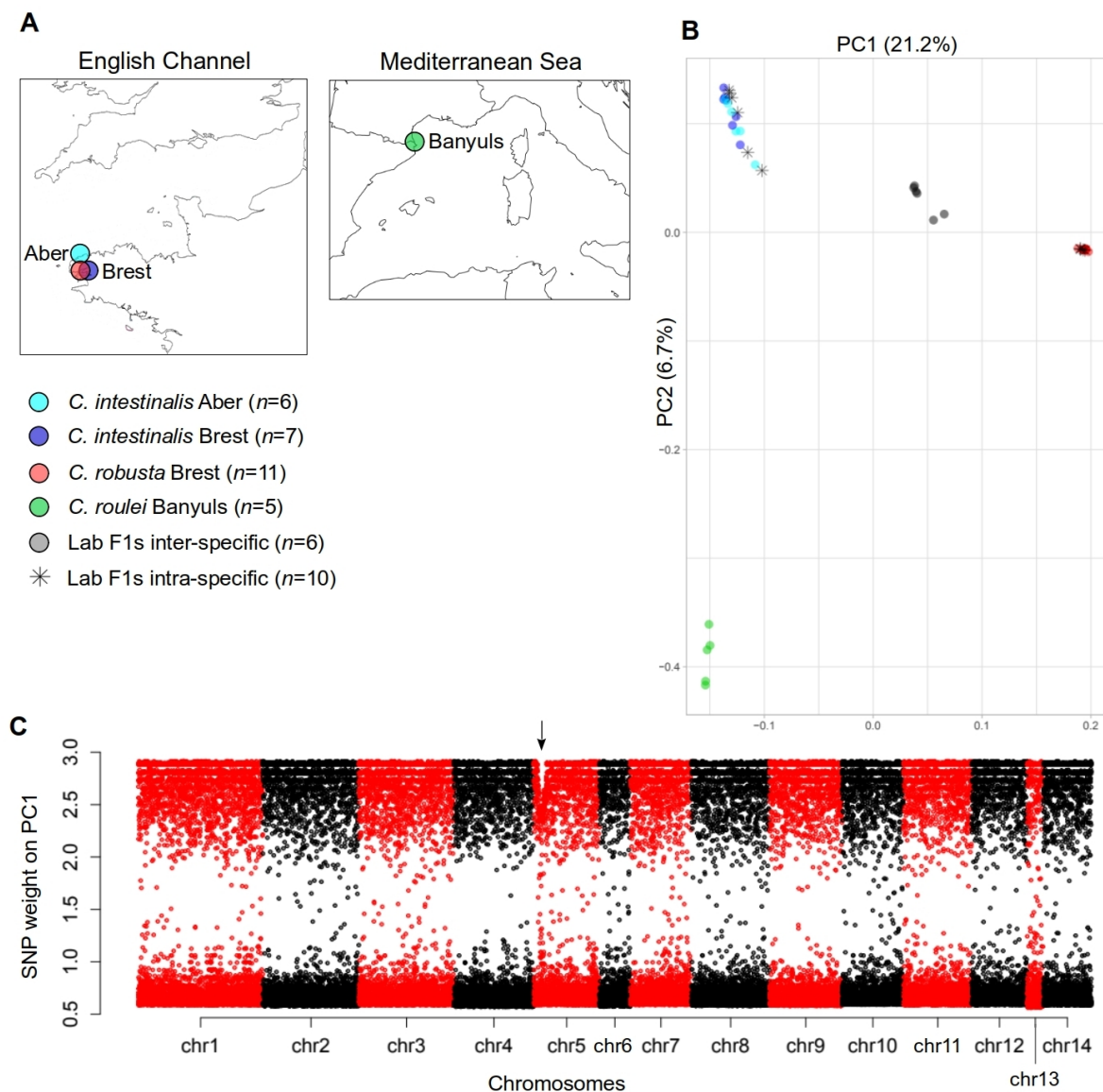
- 773 insecticides in the aphid *Myzus persicae*. *PLoS Genet.* 6:e1000999.
- 774 Racimo F, Sankararaman S, Nielsen R, Huerta-Sánchez E. 2015. Evidence for archaic adaptive
775 introgression in humans. *Nat. Rev. Genet.* 16:359–371.
- 776 Ravinet M, Yoshida K, Shigenobu S, Toyoda A, Fujiyama A, Kitano J. 2018. The genomic landscape
777 at a late stage of stickleback speciation: High genomic divergence interspersed by small localized
778 regions of introgression. *PLoS Genet.* 14:e1007358.
- 779 Robinson JT, Thorvaldsdóttir H, Winckler W, Guttman M, Lander ES, Getz G, Mesirov JP. 2011.
780 Integrative genomics viewer. *Nat. Biotechnol.* 29:24–26.
- 781 Roux C, Fraïsse C, Romiguier J, Anciaux Y, Galtier N, Bierne N. 2016. Shedding light on the grey
782 zone of speciation along a continuum of genomic divergence. *PLoS Biol.* 14:e2000234.
- 783 Roux C, Tsagkogeorga G, Bierne N, Galtier N. 2013. Crossing the species barrier: genomic hotspots of
784 introgression between two highly divergent *Ciona intestinalis* species. *Mol. Biol. Evol.* 30:1574–
785 1587.
- 786 Sabeti PC, Reich DE, Higgins JM, Levine HZP, Richter DJ, Schaffner SF, Gabriel SB, Platko JV,
787 Patterson NJ, McDonald GJ, et al. 2002. Detecting recent positive selection in the human genome
788 from haplotype structure. *Nature* 419:832–837.
- 789 Sachdeva H, Barton NH. 2018. Introgression of a block of genome under infinitesimal selection.
790 *Genetics* 209:1279–1303.
- 791 Sams AJ, Dumaine A, Nédélec Y, Yotova V, Alfieri C, Tanner JE, Messer PW, Barreiro LB. 2016.
792 Adaptively introgressed Neandertal haplotype at the OAS locus functionally impacts innate
793 immune responses in humans. *Genome Biol.* 17:246.
- 794 Sato A, Satoh N, Bishop JDD. 2012. Field Identification of ‘types’ A and B of the Ascidian *Ciona*
795 *intestinalis* in a region of sympatry. *Mar. Biol.* 159: 1611–1619.

- 796 Satou Y, Nakamura R, Deli Y, Yoshida R, Hamada M, Fujie M, Hisata K, Takeda H, Satoh N. 2019. A
797 nearly-complete genome of *Ciona intestinalis* type A (*C. robusta*) reveals the contribution of
798 inversion to chromosomal evolution in the genus *Ciona*. *Genome Biol. Evol.* 11:3144–3157.
- 799 Schmidt JM, Good RT, Appleton B, Sherrard J, Raymant GC, Bogwitz MR, Martin J, Daborn PJ,
800 Goddard ME, Batterham P, et al. 2010. Copy number variation and transposable elements feature
801 in recent, ongoing adaptation at the *Cyp6g1* locus. *PLoS Genet.* 6:e1000998.
- 802 Setter D, Mousset S, Cheng X, Nielsen R, DeGiorgio M, Hermisson J. 2020. VolcanoFinder: Genomic
803 scans for adaptive introgression. *PLoS Genet.* 16:e1008867.
- 804 Shang H, Hess J, Pickup M, Field DL, Ingvarsson PK, Liu J, Lexer C. 2020. Evolution of strong
805 reproductive isolation in plants: broad-scale patterns and lessons from a perennial model group.
806 *Philos. Trans. R. Soc. Lond. B Biol. Sci.* 375:20190544.
- 807 Shenkar N, Swalla BJ. 2011. Global diversity of Ascidiacea. *PLoS One* 6:e20657.
- 808 Shoguchi E, Kawashima T, Satou Y, Hamaguchi M, Sin-I T, Kohara Y, Putnam N, Rokhsar DS, Satoh
809 N. 2006. Chromosomal mapping of 170 BAC clones in the ascidian *Ciona intestinalis*. *Genome*
810 *Res.* 16:297–303.
- 811 Simon A, Arbiol C, Nielsen EE, Couteau J, Sussarellu R, Burgeot T, Bernard I, Coolen JWP, Lamy J-
812 B, Robert S, et al. 2020. Replicated anthropogenic hybridisations reveal parallel patterns of
813 admixture in marine mussels. *Evol. Appl.* 13:575–599.
- 814 Stachowicz JJ, Terwin JR, Whitlatch RB, Osman RW. 2002. Linking climate change and biological
815 invasions: ocean warming facilitates nonindigenous species invasions. *Proc. Natl. Acad. Sci. U.*
816 *S. A.* 99:15497–15500.
- 817 Stankowski S, Westram AM, Zagrodzka ZB, Eyres I, Broquet T, Johannesson K, Butlin RK. 2020. The
818 evolution of strong reproductive isolation between sympatric intertidal snails. *Philos. Trans. R.*

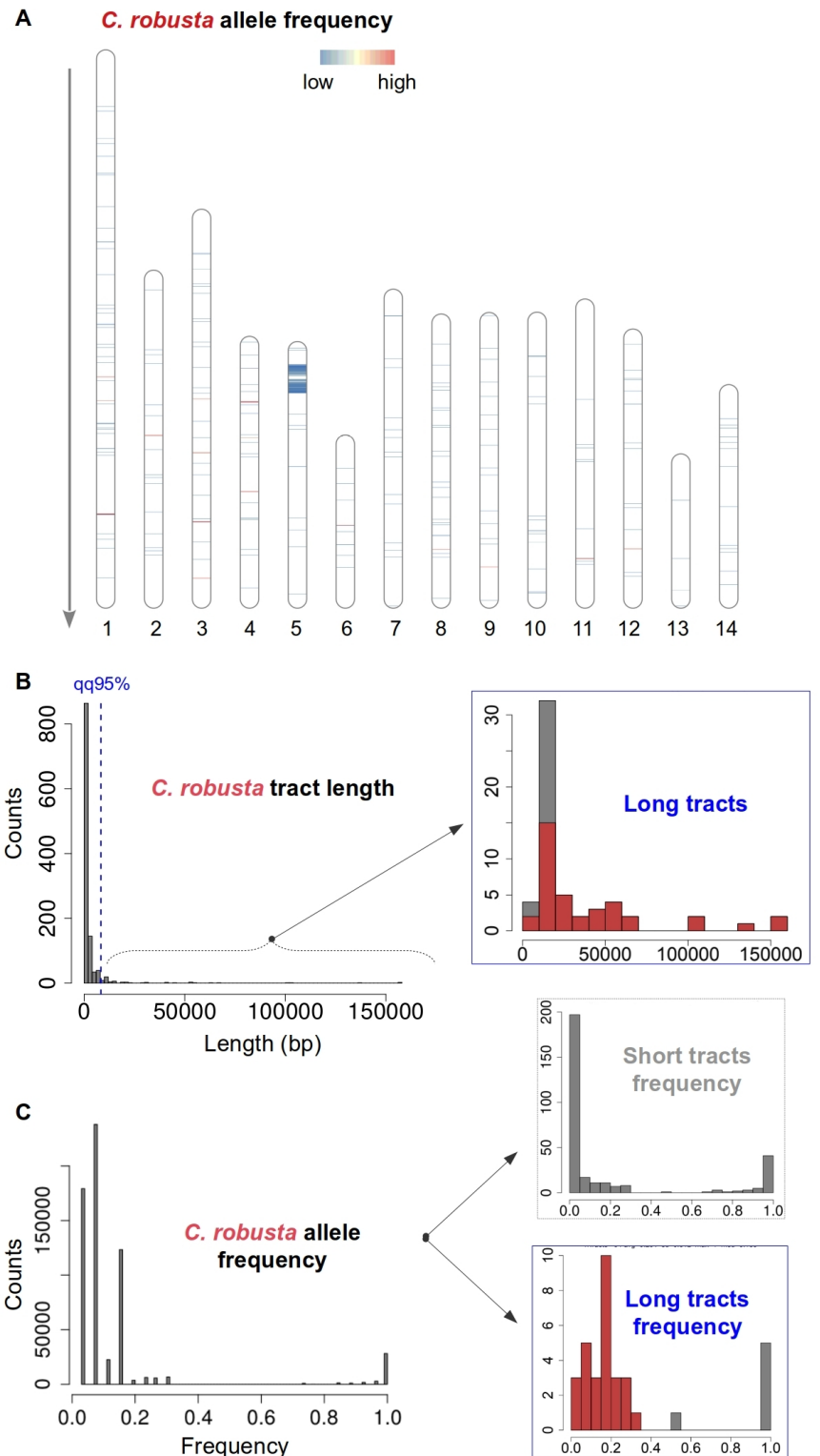
- 819 *Soc. Lond. B Biol. Sci.* 375:20190545.
- 820 Staubach F, Lorenc A, Messer PW, Tang K, Petrov DA, Tautz D. 2012. Genome patterns of selection
821 and introgression of haplotypes in natural populations of the house mouse (*Mus musculus*). *PLoS*
822 *Genet.* 8:e1002891.
- 823 Szpiech ZA. 2021. Selscan 2.0: scanning for sweeps in unphased data. *bioRxiv*. 2021.10.22.465497.
- 824 Tajima F. 1983. Evolutionary relationship of DNA sequences in finite populations. *Genetics* 105:437–
825 460.
- 826 Touchard F, Simon A, Bierne N, Viard F. 2022. Urban Rendezvous along the seashore: ports as
827 Darwinian field labs for studying marine evolution in the Anthropocene. *Evol. App.* 00:1– 20.
- 828 Tricou T, Tannier E, de Vienne DM. 2022. Ghost lineages highly influence the interpretation of
829 introgression tests. *Syst. Biol.* 71: 1147–58.
- 830 Tsagkogeorga G, Cahais V, Galtier N. 2012. The population genomics of a fast evolver: high levels of
831 diversity, functional constraint, and molecular adaptation in the Tunicate *Ciona intestinalis*.
832 *Genome Biol. Evol.* 4: 740–49.
- 833 Turissini DA, Matute DR. 2017. Fine scale mapping of genomic introgressions within the *Drosophila*
834 *yakuba* clade. *PLoS Genet.* 13:e1006971.
- 835 Valencia-Montoya WA, Elfekih S, North HL, Meier JI, Warren IA, Tay WT, Gordon KHJ, Specht A,
836 Paula-Moraes SV, Rane R, et al. 2020. Adaptive introgression across semipermeable species
837 boundaries between local *Helicoverpa zea* and invasive *Helicoverpa armigera* moths. *Mol. Biol.*
838 *Evol.* 37:2568–2583.
- 839 Van der Auwera GA, Carneiro MO, Hartl C, Poplin R, Del Angel G, Levy-Moonshine A, et al. 2013.
840 From FastQ data to high confidence variant calls: the Genome Analysis Toolkit best practices
841 pipeline. *Curr. Protoc. Bioinformatics* 43:11.10.1–11.10.33.

- 842 Viard F, Riginos C, Bierne N. 2020. Anthropogenic hybridization at sea: three evolutionary questions
843 relevant to invasive species management. *Philos. Trans. R. Soc. Lond. B Biol. Sci.* 375:20190547.
- 844 Vizzini A, Bonura A, La Paglia L, Fiannaca A, La Rosa M, Urso A, Mauro M, Vazzana M, Arizza V.
845 2021. Transcriptomic analyses reveal 2 and 4 family members of cytochromes P450 (CYP)
846 involved in LPS inflammatory response in pharynx of *Ciona robusta*. *Int. J. Mol. Sci.* 22:11141.
- 847 Weir BS, Cockerham CC. 1984. Estimating f-statistics for the analysis of population structure.
848 *Evolution* 38:1358–1370.
- 849 Wondji CS, Irving H, Morgan J, Lobo NF, Collins FH, Hunt RH, Coetzee M, Hemingway J, Ranson
850 H. 2009. Two duplicated P450 genes are associated with pyrethroid resistance in *Anopheles*
851 *funestus*, a major malaria vector. *Genome Research* 19:452–459.
- 852 Yainna S, Nègre N, Silvie PJ, Brévault T, Tay WT, Gordon K, dAlençon E, Walsh T, Nam K. 2021.
853 Geographic monitoring of insecticide resistance mutations in native and invasive populations of
854 the Fall Armyworm. *Insects* 12:468.
- 855 Yamasaki YY, Kakioka R, Takahashi H, Toyoda A, Nagano AJ, Machida Y, Møller PR, Kitano J. 2020.
856 Genome-wide patterns of divergence and introgression after secondary contact between *Pungitius*
857 sticklebacks. *Philos. Trans. R. Soc. Lond., B, Biol. Sci.* 375:20190548.
- 858 Zhan A, Briski E, Bock DG, Ghabooli S, MacIsaac HJ. 2015. Ascidiaceans as models for studying
859 invasion success. *Mar. Biol.* 162:2449–2470.
- 860 Zhan A, Macisaac HJ, Cristescu ME. 2010. Invasion genetics of the *Ciona intestinalis* species
861 complex: from regional endemism to global homogeneity. *Mol. Ecol.* 19: 4678–94.
- 862 Zimmer CT, Garrod WT, Singh KS, Randall E, Lueke B, Gutbrod O, Matthiesen S, Kohler M, Nauen
863 R, Davies TGE, et al. 2018. Neofunctionalization of duplicated P450 genes drives the evolution
864 of insecticide resistance in the Brown Planthopper. *Curr. Biol.* 28:268–274.e5.

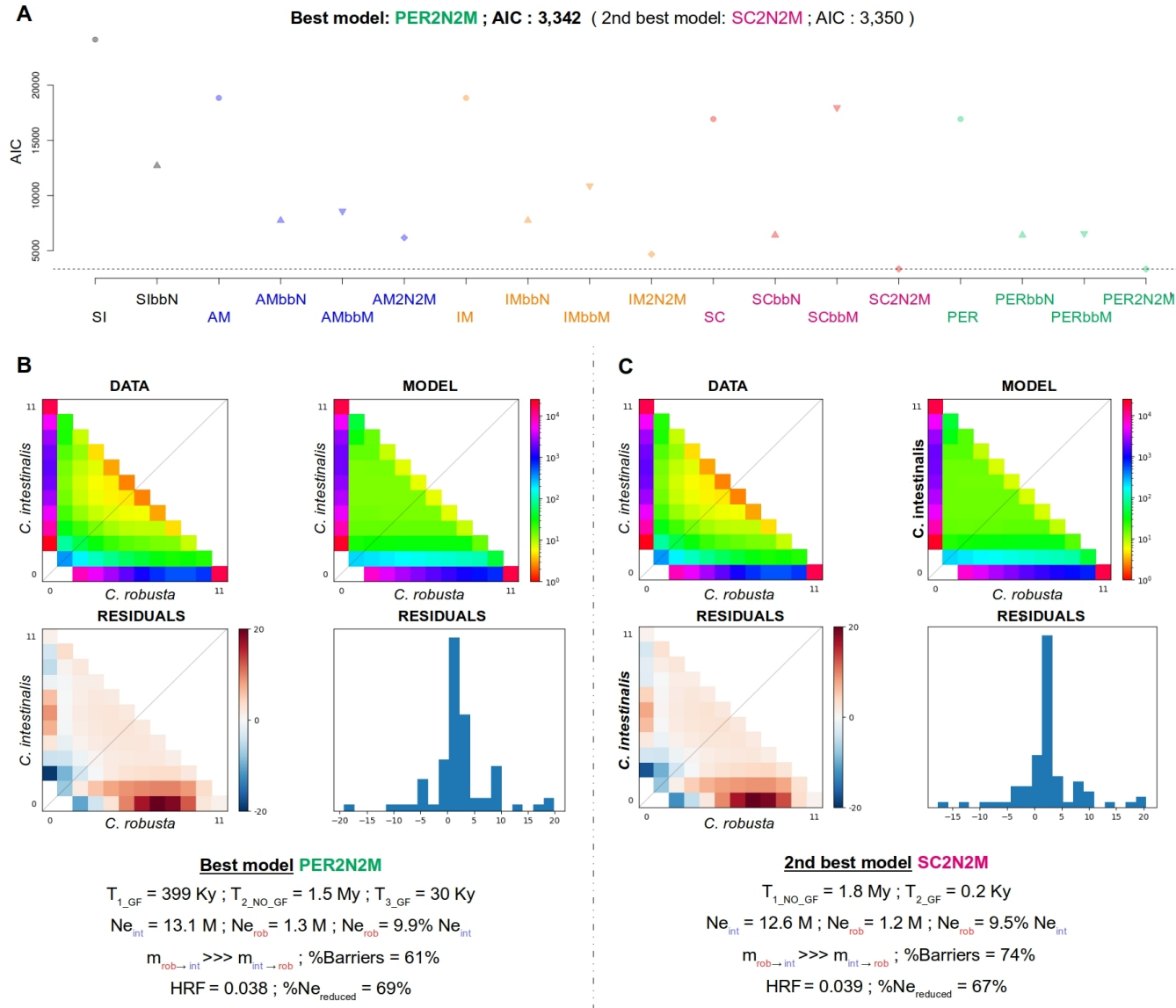
865 **Figure 1** Genetic population structure. **A.** Geographical location of the samples in the English Channel and
866 Iroise Sea (*C. robusta* and *C. intestinalis*) and the Mediterranean Sea (*C. roulei*). Numbers in brackets refer to the
867 sample size of each population. “Lab F1s” indicates the intraspecific and interspecific offspring produced in the
868 laboratory. Further information on samples is provided in **Table S1**. The color code (*C. robusta* in red, *C.*
869 *intestinalis* in blue and *C. roulei* in green) is used throughout the manuscript. **B.** Principal Component Analysis
870 of 45 individuals genotyped at 194,742 unlinked SNPs (pruning threshold: $r^2 > 0.1$). Numbers in brackets refer to
871 the proportion of variance explained by each axis. Three poorly sequenced parents were removed from the
872 analysis (see **Table S1**). **C.** SNP weights to the first axis of the PCA (after removing the SNPs contributing less
873 than the 75th quantile of the weight distribution). The introgression hotspot on chromosome 5 is highlighted with
874 an arrow. Dataset #1 “phased SNPs with offspring” was used.



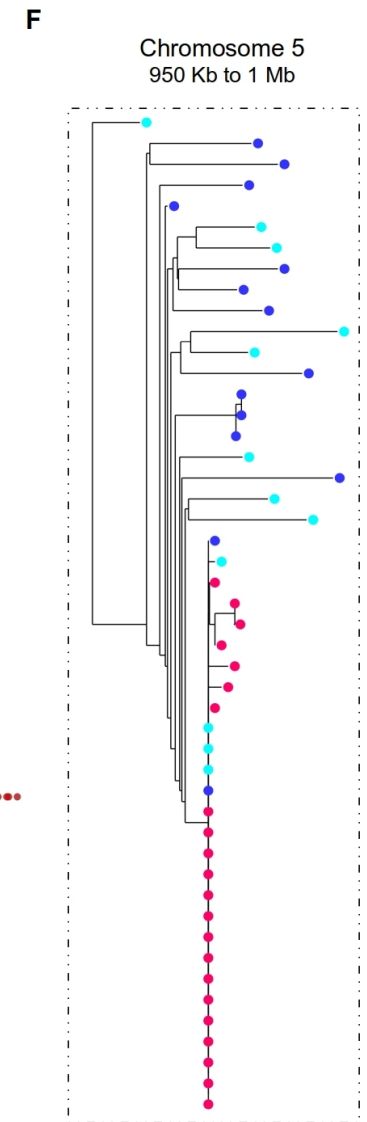
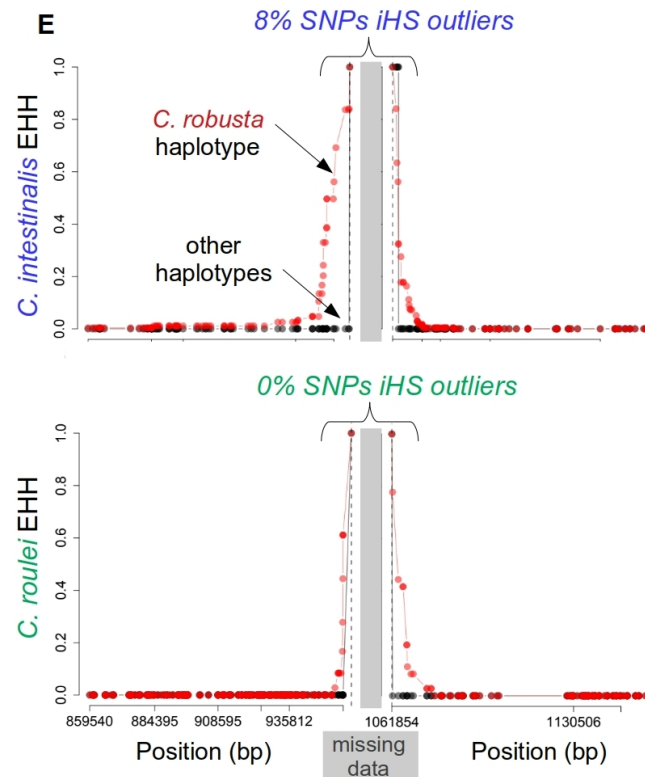
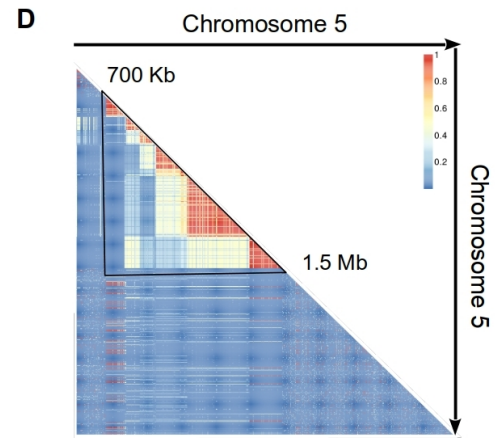
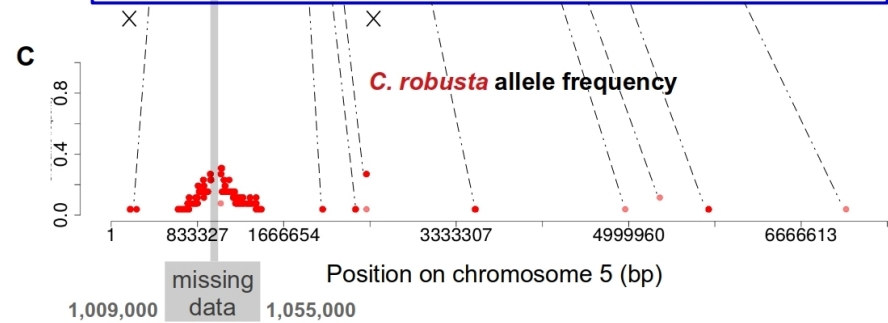
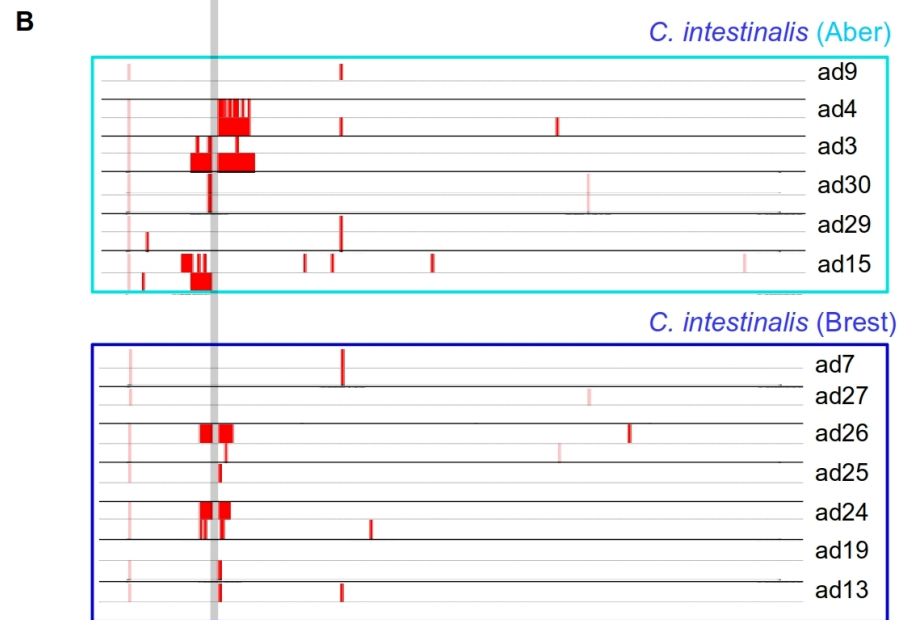
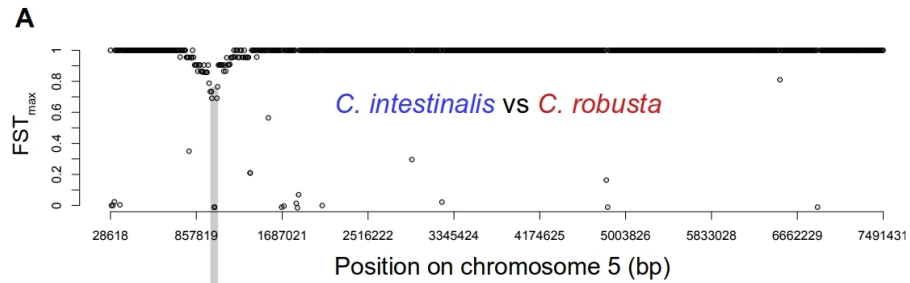
875 **Figure 2** Local ancestry patterns of the *C.*
 876 *intestinalis* genomes sampled in the English
 877 Channel and Iroise Sea using 640,044 phased
 878 SNPs. *C. robusta* and *C. roulei* were used as
 879 the donor populations. **A.** Physical mapping
 880 across the 14 chromosomes of the frequency
 881 of the *C. robusta* tracts introgressed into *C.*
 882 *intestinalis*. The color gradient (blue to yellow
 883 to red) follows the gradient in allele frequency
 884 from low (0.038) to high (1.0); regions in
 885 white correspond to null introgression. The
 886 direction of the arrow indicates the coordinate
 887 direction from top (start) to bottom (end). The
 888 R package RIdiograms was used for the
 889 plotting. **B.** Length distribution of the *C.*
 890 *robusta* introgressed tracts ($n=1,143$ tracts).
 891 The maximum tract length is 156 Kb, the
 892 average is 2.6 Kb, and the median is 0.38 Kb.
 893 A blue dashed line depicts the 95th quantile of
 894 the length distribution (8.3 Kb), and it was
 895 used as a threshold to delineate long tracts. A
 896 total of 38 of 57 long tracts were detected on
 897 chromosome 5 (red portion of each bar). **C.**
 898 Allele frequency of the SNPs lying on the *C.*
 899 *robusta* introgressed tracts ($n=621,249$
 900 variants). The maximum frequency is 1, the average is 0.14, and the median is 0.08. On the right, the frequency
 901 of variants lying on short tracts (upper panel) or long tracts (lower panel) is depicted. The red portion of each bar
 902 indicates the tracts on chromosome 5. Allele frequency was calculated, excluding any position with missing data.
 903 Dataset #3a “phased SNPs” was used.



904 **Figure 3** Inference of the divergence history between *C. robusta*
 905 and *C. intestinalis* with moments. **A.** AIC value of the best run for
 906 each model. **B.** Observed site frequency spectrum (SFS), modeled
 907 SFS and residuals of the best model. Maximum likelihood values of
 908 the parameters are provided. **C.** Same as in **B** but for the second-best
 909 model. Analyses were based on the folded SFS after LD-pruning the
 910 SNPs. Five demographic scenarios were modeled: SI = strict
 911 isolation, IM = isolation with continuous migration, SC = secondary
 912 contact, AM = ancient migration, PER = periodic connectivity.
 913 Different versions of these scenarios were tested: bbN = genomic
 914 heterogeneity of the effective population sizes, bbM = genomic
 915 heterogeneity of the effective migration rates, 2N2M = both types of
 916 heterogeneities, “” = no heterogeneities. Five replicates were run for
 917 each model. Parameters are as follows: T = times in years, assuming
 918 two generations per year in European waters (the “GF” label refers to
 919 gene flow), N_e = effective population sizes in numbers of
 920 individuals, m = migration rates (direction given by the arrow),
 921 %Barriers = proportion of the genome with null migration, % $N_{e_{reduced}}$
 922 = fraction of the genome experiencing reduced N_e , HRF = factor by
 923 which N_e is reduced. Full details are provided in **Table S3**. Dataset #5 “all SNPs without missing data” was used, excluding chromosome 5.



924 **Figure 4** Analyses of the introgression hotspot on chromosome 5. **A.** Maximum F_{ST} between *C. robusta* and *C.*
925 *intestinalis* was calculated in non-overlapping 10 Kb windows along chromosome 5. Windows with less than 10
926 SNPs were excluded. The x-axis is in bp. **B.** Haplotypes of the *C. intestinalis* individuals in the two sampled
927 localities (sample IDs are depicted on the right, see **Table S1**). Each individual displays two haplotypes
928 delimited by horizontal lines. The *C. robusta* introgressed tracts are shown as red bars. The white background
929 represents the non-introgressed tracts and missing data. The tract boundaries were determined based on the
930 ancestry probability of each position, as shown in **Figure S7**. **C.** Frequency of the *C. robusta* alleles lying on the
931 introgressed tracts along chromosome 5. Allele frequency was calculated, excluding any position with missing
932 data (e.g., the nearly fixed SNP at position 28,801 bp on panel **B** was excluded and designated with the first cross
933 on panel **C**). The grey horizontal band running through all panels refers to the “missing data region” (due to high
934 coverage) in the core region of the hotspot (from 1,009,000 to 1,055,000 bp). **D.** Linkage disequilibrium pattern
935 between the 111,951 SNPs fixed between *C. robusta* and *C. roulei*. The color scale indicates the level of LD
936 from blue (low) to red (high). **E.** Haplotype-based selection test using *SelScan*. EHH is shown for the *C. robusta*
937 haplotype (red) and the other haplotypes (black) in *C. intestinalis* (upper panel) and *C. roulei* (lower panel) using
938 a 100 Kb maximal extension. A separate analysis was done on the left and right of the “missing data region”
939 (grey band) using the most frequent *C. robusta* allele closest to the grey band as target SNP. Absolute iHS was
940 calculated based on the EHH results and normalized in windows of 50 Kb. The threshold value of the normalized
941 iHS was set to 3 (which refers to the 99th quantile). **F.** Neighbor-joining tree of a 50 Kb window to the left of the
942 “missing data region” at the center of the chromosome 5 hotspot. Colored dots are red, dark blue and light blue
943 for individuals of *C. robusta*, *C. instestinalis* from Brest and *C. intestinalis* from Aber, respectively. Dataset #2
944 “**all SNPs with missing data**” was used for the F_{ST} , #3a “**phased SNPs**” for Chromopainter haplotypes, #3c
945 “**FASTA version of phased SNPs**” for the NJ tree and #4 “**ancestry informative phased SNPs**” for the LD
946 triangle.



947 **Figure 5** Copy number variation at two candidate SNPs on the cytochrome P450 family 2 subfamily U gene.
948 The two SNPs (labeled with their position in bp) lie in the “missing data region” of the introgression hotspot on
949 chromosome 5. Candidates were defined as having a variant allele fraction, VAF \leq 50% in *C. intestinalis*, a
950 VAF \geq 90% in *C. roulei* and a VAF \leq 10% in *C. robusta*. No candidates were found in the other direction (i.e.
951 with the minor VAF in *C. roulei*). Copy number at each SNP was calculated as its allele read depth normalized
952 by the per-site read depth averaged across all sites (excluding sites with less than ten reads) for each individual
953 (labeled on the left). A copy number of one (vertical dashed line) means that the SNP lies on a single-copy locus.
954 Values for the *C. robusta* allele (red) and the *C. intestinalis* allele (blue) are separately shown. Read depth was
955 obtained from the bam files. Horizontal dashed lines separate the different species, and *C. intestinalis* individuals
956 introgressed at the hotspot (see **Figure 4**) were labeled as “introgressed”. Dataset #7 “unfiltered mapping files”
957 was used.

